REPORT DOCUMENTATION PAGE

Form Approved
OMB No. 0704-0188

1. REPORT DATE *(DD-MM-YYYY)*	2. REPORT TYPE	3. DATES COVERED *(From – To*
17-Feb-2005	Journal Article	1-Oct-2003 – 30-Sep-2004

4. TITLE AND SUBTITLE

Intervalence Band Absorption and Carrier Heating In Type-II Sb-Based Lasers

5a. CONTRACT NUMBER

5b. GRANT NUMBER

5c. PROGRAM ELEMENT NUMBER
(1) 61102F (2) 63605F

6. AUTHOR(S)

Dr. Vern Schlie, Ahmed I. Lobad

5d. PROJECT NUMBER
(1) 2305 (2) 4866

5e. TASK NUMBER
(1) LY (2) LY

5f. WORK UNIT NUMBER
(1) 01 (2) 01

7. PERFORMING ORGANIZATION NAME(S) AND ADDRESS(ES)

8. PERFORMING ORGANIZATION REPORT NUMBER

9. SPONSORING / MONITORING AGENCY NAME(S) AND ADDRESS(ES)

AFRL/DELS
3550 Aberdeen Ave SE
Kirtland AFB NM 87117-5776

10. SPONSOR/MONITOR'S ACRONYM(S)

11. SPONSOR/MONITOR'S REPORT NUMBER(S)

12. DISTRIBUTION / AVAILABILITY STATEMENT
Approved for public release; distribution is unlimited.

13. SUPPLEMENTARY NOTES
Journal article accomplished for two different efforts listed in Blocks 5c thru 5f above.

14. ABSTRACT

The intervalence absorption in InAs/InGaSb/InAs type-II 4μm quantum well laser structure was investigated using band-edge nonlinear pump-probe spectroscopy techniques where two pump beams chopped at different frequencies are used to excite the sample. The spectrally resolved probe nonlinearity is measured at the sum frequency. Given their different characteristic nonlinearities, the contribution of the intervalence absorption process (IVA) was resolved from that of the interband gain dynamics. The IVA absorption occurs at in-plane momentum k11~0.025 $Å^{-1}$and is not resonant with the interband lasing energy, therefore does not compete with the interband transition at low temperature and low carrier densities. A density dependent interband transition matrix element of $N^{0.17}$was deduced reflecting the enhancement of the electron hole wavefunction overlap due to the space-charge fields in the type-II wells. Significant lattice heating observed above 80K is reflected in the growth of an out of phase slow signal, resulting from the reduction of lattice thermal conductivity and the IVA resonance enhanced nonradiative Auger recombination transitions at higher temperatures. Thermal diffusion times of the order of ~ 100 μs that increases with temperature were measured.

15. SUBJECT TERMS
Quantum wells, pump-probe diagnostics, mid-IR semiconductor materials

16. SECURITY CLASSIFICATION OF:			17. LIMITATION OF ABSTRACT	18. NUMBER OF PAGES	19a. NAME OF RESPONSIBLE PERSON
a. REPORT	b. ABSTRACT	c. THIS PAGE			Dr. Vern Schlie
Unclassified	Unclassified	Unclassified	Unlimited	20	19b. TELEPHONE NUMBER *(include area code)* (505) 853-3440

Intervalence band absorption and carrier heating in type-II Sb-based lasers

Ahmed I. Lobad and L.A. (Vern) Schlie

Air Force Research Laboratory, Directed Energy Directorate (AFRL/DEL)
3550 Aberdeen Ave, SE, Kirtland AFB, NM 87117

ABSTRACT

The intervalence absorption in InAs/InGaSb/InAs type-II 4 μm quantum well laser structure was investigated using band-edge nonlinear pump-probe spectroscopy techniques where two pump beams chopped at different frequencies are used to excite the sample. The spectrally resolved probe nonlinearity is measured at the sum frequency. Given their different characteristic nonlinearities, the contribution of the intervalence absorption process (IVA) was resolved from that of the interband gain dynamics. The IVA absorption occurs at in-plane momentum $k_{\|} \sim 0.025$ Å^{-1} and is not resonant with the interband lasing energy, therefore does not compete with the interband transition at low temperature and low carrier densities. A density dependent interband transition matrix element of $N^{0.17}$ was deduced reflecting the enhancement of the electron hole wavefunction overlap due to the space-charge fields in the type-II wells. Significant lattice heating observed above 80 K is reflected in the growth of an out of phase slow signal, resulting from the reduction of lattice thermal conductivity and the IVA resonance enhanced nonradiative Auger recombination transitions at higher temperatures. Thermal diffusion times of the order of ~ 100 μs that increases with temperature were measured.

Introduction

Type-II quantum well (QW) antimonide based MIR lasers have advanced rapidly since their first demonstration in 1994 [1], with peak power outputs reaching 5 W at low temperatures [2]. However their performance at high temperatures fall short of theoretical expectations. Ongstad *et al.* investigated the effect of indium content in strained InAs/$In_xGa_{1-x}Sb$/InAs active layers [3]. They measured an improvement in the characteristic temperature and differential quantum efficiency with increased indium content and attributed the improvement to the onset and enhancement of hole confinement in the InGaSb layers. Intervalence band absorption (IVA) that is resonant with the interband lasing energy has been suggested to be the culprit for the high internal losses at higher temperatures [4]. More recent results though suggest that no significant loss increase due to IVA is observed and that the poor thermal performance is due to Auger processes and the large difference between the conduction and valence in-plane curvatures [5].

The IVA absorption cross section is masked by the stronger valence-conduction interband gain transition and has so far been estimated from band structure calculations and indirectly deduced from external quantum efficiency measurements. To resolve the intervalence absorption process we employed a nonlinear pump-probe technique where two pump beams modulated at different frequencies excite the sample and the spectrally resolved probe nonlinearity is measured at the sum frequencies. We have previously shown that the magnitude and signature of the nonlinear signal can be used to determine position of the quasi Fermi energy and the carrier temperature in semiconductors [6]. This technique was also used to investigate the coherent phonon generation mechanism in solids and distinguish between impulsive and displacive processes [7].

After describing the sample and setup, the nonlinear pump-probe technique and the nonlinear response of a thermal carrier distribution at different temperatures are discussed. The density dependence of the interband transition matrix element is then deduced from the measured nonlinear spectra as a function temperature. The intervalence absorption was resolved from simultaneous fitting of the linear and nonlinear spectra at 10 K for different carrier densities. Finally excessive carrier and lattice heating for lattice temperatures above 80 K is discussed showing evidence reduced thermal diffusion rates and increasing Auger rates at higher temperatures.

Sample and Setup

The QW laser sample has a characteristic temperature of 48 K and incorporates 6 type-II quantum wells separated by a 1000 Å thick integrated absorber quaternary region latticed matched to the GaSb substrate. Each well has a W-structure comprised of 24 Å thick $In_{0.25}Ga_{0.75}Sb$ hole well sandwiched by two 21 Å InAs electron wells [3]. This amounts to ~ 40 nm effective width of the active region. Empirical pseudopotential method (EPM) [8] was used to determine the conduction and valence effective masses and band nonparabolicities. EPM calculation suggests that for this indium concentration the hole wave function is confined in the InGaSb layer as opposed to being delocalized in the quaternary integrated absorber region. The conduction band has an in-plane electron mass of $m_{e\|} \approx 0.035m_o$ with a nonparabolicity of α_e ~1.4, the valence band has an in-plane hole mass of $m_{h\|} \approx 0.14m_o$ with a nonparabolicity α_h~4.5 [9]. The energy levels in these structures are inhomogenously broadened due to InAs-GaSb interface roughness of 1 mono-layer [10]. To account for this broadening, the simulated spectra were convolved with a 7 meV FWHM Gaussian function.

We used an 80 MHz Ti:Sapphire pumped periodically poled lithium niobate (PPLN) OPO producing ~ 150 *fs* tunable idler pulses at ~ 4 μm and signal pulses ~ 1μm. Two signal pump pulses were used to excite carriers and the gain spectra dynamics was measured with the tunable idler probe. The pump polarizations are parallel (Pu1 || Pu2) and are both perpendicular to the probe polarization. The two pumps are temporally delayed by less than a pico-second to avoid generating a carrier spatial grating [6]. All spectra were recorded at a probe time delay of 250 ps from the two pumps. This delay is long enough to insure carrier thermalization to the lattice temperature while much shorter than the ~ 6 ns recombination time at 10 K. Following carrier generation in the integrated absorber region they cool, diffuse to and collect in the QWs with a time constant of ~ 20 ps. The pump pulses are focused to a 180 μm spot size and the probe is focused to a 70 μm spot size. The average pump fluences used in this work ranges from 20 to 120 Wcm^{-2} and the estimated carrier density accumulating in the wells varies in the range 2 to 7 $x10^{11}$ cm^{-2}. The highest fluence is denoted as Pu_o below. Since the sample in not cleaved as a laser structure we can exceed the carrier density at threshold. Measurements were done at temperatures ranging from 10 K to 300 K, the epitaxial side of the sample (laser side) was pressed against the cold finger and silver paint was used to insure good thermal contact. To measure the full spectral range covered by the carrier distribution (≤ 60 meV) the probe (idler) was tuned by adjusting the OPO cavity length with a PZT. The total spectral range can be covered by tuning the probe and measuring three separate partially overlapping spectra. This slight tuning did not drastically affect the OPO output. Slight changes in the pump power (~ 10%) were compensated with neutral density filters. The measured spectra were normalized with the probe spectra. The spectral response of the combined spectrometer/detector system was determined using a black body source and used to correct the measured spectra.

Nonlinear Pump-Probe

The linear (ΔT) and nonlinear (ΔT_{nl}) transmission changes are given by,

$$\Delta T(N,\varepsilon) = \alpha_{cv}(N)\,[f_e(N,\varepsilon) + f_h(N,\varepsilon)]^* C(\varepsilon) - \alpha_{IVA}(\varepsilon) f_h(N,\varepsilon) \quad (1)$$

$$\Delta T_{nl}(N,\varepsilon) = \Delta T(N,\varepsilon) - 2\Delta T(N/2,\varepsilon) \quad (2)$$

where, f_e and f_h are the electron and hole Fermi functions and α_{cv}, α_{IVA} are the conduction-valence interband and the intervalence optical transition strengths respectively. We used a type-I QW Coulomb enhancement factor given by $C(\varepsilon) = \exp(\pi/\sqrt{\Delta}) \Big/ \cosh(\pi/\sqrt{\Delta})$, where $\Delta = (\varepsilon - \varepsilon_g)/\varepsilon_{ex}$ and the exciton energy was taken to be ε_{ex}= 2 meV. The interband matrix element was taken to be carrier-density-dependent to account for the type-II nature of these wells where charge separation of the injected carriers induces band bending that increases the electron-hole wave function overlap and the optical transition strength.

In a lock-in measurement with two excitation modulation frequencies, a signal's nonlinearity is split among a dc term, the two fundamental modulation frequencies, their sum and difference frequencies. The rms signals measured at the fundamental and sum frequencies are given by,

$$Signal_{@\, f_{in}, f_{out}} \sim \left(\frac{\Delta T}{2} + \frac{\Delta T_{nl}}{4}\right) \Big/ \sqrt{2} \quad ; \quad Signal_{@\, f_{sum}} \sim \frac{\Delta T_{nl}}{9} \quad (3)$$

The nonlinear signature of the interband filling contribution consists of a negative contribution (saturating-sublinear behavior) close to the band edge that crosses to a positive contribution (superlinear behavior) at an excess energy E_{cr}. At low temperatures where the Fermi energy is larger than the Fermi edge thermal smearing ($E_f >> 2\ k_B T$), E_{cr} is at the Fermi energy

E_{f1} produced by one pump pulse and the nonlinear spectrum is symmetric around that point. As the Fermi edge thermal smearing increases, the nonlinear spectrum becomes less symmetric and the crossing energy increases. Assuming a density independent matrix element one can solve the following equation,

$$f(E_{cr},E_{f2}(N),T)-2f(E_{cr},E_{f1}(N/2),T)=0 \tag{4}$$

to obtain,

$$E_{cr}=E_{f1}+k_BT*\ln(\frac{1}{1-2\exp[-(E_{f2}-E_{f1})/k_BT]}) \tag{5}$$

where f is the Fermi function and E_{f1}, E_{f2} are the Fermi energies for injected carriers $N/2$ (one pump) and N (both pumps) respectively. The Fermi energy in a QW of density of states D is given by $E_f(N,k_BT)=k_BT*\ln[\exp(N/Dk_BT)-1]$, which in the high temperature limit tends to $\lim_{T\to\infty}E_f\to k_BT*\ln(\frac{N}{Dk_BT})$ and the Fermi energy difference tends to $\lim_{T\to\infty}(E_{f2}-E_{f1})\to k_BT*\ln(2)$. As the temperature increases, the Fermi energy E_{f1} decreases and goes below the band gap for a nondegenerate distribution, but the second term in Eq. (5) increases and diverges for E_{f2} - $E_{f1}=k_BT*\ln(2)$ more than offsetting the decrease in E_{f1}.

Results and Discussion

In Fig. 1 we show the nonlinear spectra plotted for different lattice temperatures at low carrier injection. It will be shown later that the IVA transition is not resonant with the band edge and does not occur at $k_{||}$=0, therefore its contribution can be ignored for low carrier injection and low excess energies. The crossing energies (E_{cr}) for the spectra of Fig.1 are plotted in Fig. 2. They do not increase with temperature as expected from Eq. 5. Also displayed in Fig. 2 are the

calculated crossing energies for a density independent matrix element and for a matrix element proportional to $N^{0.17}$ taking into account the electron and hole distributions. A carrier density dependent interband matrix element is clearly required to fit the measured data in accord with what is expected for a type-II QW. In their modeling of Sb-based type-II quantum cascade lasers, Liu *et al.* found that the carrier induced screening field results in a 10% gain increase for a carrier density of 10^{18} cm^{-3} in comparison to a flat band model where the field is not accounted for [11]. This screening field also results in an energy blue shift that counters the many-body-induced red shift of the gain spectrum.

The linear and nonlinear spectra measured at 10 K for three injected densities (Pu_o, $Pu_o/2$ and $Pu_o/5$) are plotted in Fig. 3. The thin line traces are the simulated spectra taking into account only the interband transition (α_{cv}). The simulation matches well (deviates from) the measured spectra below (above) 0.33 eV for both the linear and nonlinear spectra. This suggests that the intervalence absorption is not resonant with the band edge and is expected to be significant only above 0.34 eV. To account for the deviation in the high-energy side of the measured and simulated spectra we assume the following simplified IVA form,

$$\alpha_{IVA} \exp(-[\frac{E - E_{IVA}}{\Delta_{IVA}}]^2) * [1 + \exp(\frac{E_{fh} - E_o}{k_B T})]^{-1} \qquad (5)$$

where α_{IVA} is the intervalence transmission matrix element, E_{IVA} is the energy resonance between the upper valence band and the lower valence band where the absorption originates, Δ_{IVA} is the energy width of that resonance, the second term is the hole Fermi function. The hole Fermi energy E_{fh} determines the available density of empty hole states in the upper valence band for intervalence absorption at an excess hole energy E_o. Naturally E_o determines the in-plane momentum $k_{||}$ value where the intervalence absorption resonance takes place. A schematic figure

of the band structure showing the intervalence and interband transitions are presented in Fig. 4. The parameters E_{IVA} and Δ_{IVA} are roughly determined from the position of maximum deviation between the measured and interband-only simulated spectra. In addition, only a unique set values for α_{IVA} and E_o are capable of simultaneously accounting for the magnitude of the deviation in the linear and nonlinear spectra according to Eqs. (1) and (2). The dotted traces represents the simulation taking into account both the intervalence and interband contributions resulting in a much better fit throughout the measured range for both spectra. The parameters used to fit the spectra are $\alpha_{cv} \sim 2000$ cm^{-1}, $\alpha_{IVA} \sim 20000$ cm^{-1}, $E_o \sim$ -16 meV ($k_{||} \sim 0.025$ Å^{-1}), $E_{IVA} \sim 0.345$ eV, $\Delta_{IVA} \sim 0.013$ eV. The injected carrier density in the wells was found to saturate with incident powers as $N[Pu] \propto \frac{Pu}{1+Pu/(1.6Pu_o)}$, it is possible that this saturation is due to the limited confinement depth of the quantum wells leading to carrier detrapping from the wells. For better fit, a carrier heating of ~ 10 K per pump pulse was assumed. This is consistent with observed slow cooling and residual heating for carrier temperatures below the optical phonon temperature [12].

Using the intervalence absorption parameters we estimate an absorption/loss of ~ 400 cm^{-1} at Pu=Pu_o. Though this large value does not affect lasing at low temperatures since the IVA transition is not resonant with the interband transition in either in-plane momentum or energy. In a lasing situation the total carrier density is clamped at about $Pu_o/5$ where the hole population at $E_h = E_o$ is negligible. At higher temperatures the hole population at E_o increases along with the IVA transitions. In a laser operation this absorption is not only a passive internal loss mechanism since it also causes heating of the holes that clamps intracavity lasing power. In addition a significant hole population at E_o leads to resonance enhancement of the Auger process, which

further increases carrier heating. In fact, luminescence correlation (excitation correlation) measurements point to a sharp drop in the carrier lifetime from 6 ns at 10 K to 1 ns at 150 K at a density equivalent to $Pu_o/2$.

For $Pu \geq Pu_o/2$, the curve fitting starts to deteriorate above 80 K with indications of both excess carrier and lattice heating in excess of 50 K per excitation pulse at 150 K. Carrier heating is reflected in the slope of the linear spectrum high energy tail. Lattice heating is deduced from the appearance and growth of an out phase (quadrature) signal measured at chopping frequencies of the order of 2 KHz. This indicates the presence of a slow signal that builds up and decays with a time constant of the order of 100's of μs time scale suggesting a lattice heating effect. The quadrature signal is not measurable at 10 K. The in-phase and quadrature signals are plotted in Fig. 5 for temperatures 80 K (a) and 180 K (b). At 180 K the quadrature signal is larger than the in-phase signal that represents the carrier contribution. In principle, the slow signal can contribute to both the in-phase and quadrature signals according to its phase that is determined by its time constant. This slow signal develops from heating modulation and its effect on the dielectric constants possibly through modulating the strain in the heterostructure and therefore the band structure. We directly measured the buildup and recovery of the heating contribution for different lattice temperatures by averaging the transmission signal. The traces, shown in Fig. 6, were acquired at negative time delay (probe preceding the pump) and at ~ 50 meV above the band edge to preclude any carrier contributions. The inset shows the variation of the extracted thermal diffusion time constant as a function of the lattice temperature. The values of the diffusion time constant suggest a radial diffusion process where the time constant is proportional to the excited area and inversely proportional to the thermal conductivity. The average thermal conductivity for the QW well constituents decreases from ~ 15 $W.cm^{-1}.K^{-1}$ at 20 K to ~ 0.3

$W.cm^{-1}.K^{-1}$ at 300 K [13]. Using these values we estimate an average radial diffusion times of 5 μs at 20 K and 125 μs at 300 K. These estimates are smaller than those measured in the inset of Fig. 6. This discrepancy could be attributed to the effect of interface roughness on the radial thermal conductivity in nanoscale heterostructures [14]. The growth of the thermal signal with lattice temperature is related to the decrease of the thermal conductivity rates along with the increase in the nonradiative recombination rates. As noted before, no slow thermal signal is measured at 10 K lattice temperature despite the fact that a 10 K heating per pulse was deduced from curve fitting of the linear and nonlinear spectra (Fig.3). Therefore it is reasonable to conclude that the measured heating at higher lattice temperatures exceeds 50 K per pulse. This excess heating resulting from increased nonradiative recombination and decreased thermal conductivity more than compensates for increases in the lattice and carrier heat capacities with temperature. Thermal diffusion along the growth direction should be orders of magnitude faster than the radial diffusion due to the much stronger thermal gradient in that direction. Estimating the thermal diffusion time along the growth direction requires knowledge of the thermal resistance along various interfaces in the heterostructure. To avoid this heating buildup, laser operation is usually limited to 32 μm pulses of 1% duty cycle [2]. At the lasing threshold for lattice temperature of 180 K, the average power density (average power) used in Ref. [2] is the same magnitude as (~14 times greater than) that used in this work at 50% duty cycle. We note that persistent heating in excess of 50 K lasting for hundreds of picoseconds has been observed in luminescence measurements in narrow-band-gap superlattices [15].

Conclusion

A nonlinear pump-probe technique was used to characterize the intervalence absorption in Sb-based QW MIR lasers. A density dependent interband transition matrix element of $N^{0.17}$ was deduced reflecting the enhancement of the electron hole wavefunction overlap due to the space-charge fields in the type-II wells. The IVA absorption occurs at in-plane momentum $k_{||}$=0.02 $Å^{-1}$ and therefore does not compete with the interband transition at low temperature and low carrier densities. Accumulated carriers in the well have a saturation sheet density of $1.5x10^{12}$ cm^{-2}. Significant lattice heating above 80 K is reflected by the growth of an out of phase slow signal. Carrier and lattice heating are in excess of 50 K per pulse at 150 K lattice temperature. This heating results from the reduction of lattice thermal conductivity and the IVA resonance enhanced nonradiative recombination at higher temperatures. Thermal diffusion times of the order of ~ 100 μs that increases with temperature were deduced.

Acknowledgement

We thank Dr. R. Kaspi for providing the laser samples. This research was supported by the Air Force Office of Scientific Research (AFOSR).

References

[1] R.H. Miles, D.H. Chow, Y.-H Zhang, P.D. Brewer, R.G. Wilson, Appl. Phys. Lett. **66**, 1921 (1995).

[2] R. Kaspi, A.P. Ongstad, G.C. Dente, J. Chavez, M.L. Tilton, and D. Gianardi, Appl. Phys. Lett. **81**, 406 (2002).

[3] A.P. Ongstad, R. Kaspi, J.R. Chavez, G.C. Dente, M.L. Tilton, and D.M. Gianardi, J. Appl. Phys. **92**, 5621 (2002).

[4] W.W. Bewley, I. Vurgaftman, C.L. Felix, J.R. Meyer, C.-H. Lin, D. Zhang, S.J. Murry, S.S. Pei, and L.R. Ram-Mohan, J. Appl. Phys. **83**, 2384 (1998); H.Q. Le, C.H. Lin, S.J. Murray, R.Q. Yang, and S.S. Pei, IEEE J. Quantum Elect. **34**, 1016 (1998).

[5] S. Suchalkin, D. Westerfeld, D. Donetski, S. Luryi, G. Blenkey, R. Martinelli, I.Vurgaftman, and J. Meyer, Appl. Phys. Lett. **80**, 2833 (2002); A.P. Ongstad, R. Kaspi, C.E. Moeller, M.L. Tilton, J.R. Chavez, and G.C. Dente J. Appl. Phys. **95**, 1619 9 (2004).

[6] A. Lobad, and L.A. Schlie, J. Appl. Phys. **95**, 97 (2004).

[7] A.I. Lobad and A.J. Taylor, Phys. Rev. B *Rapid Comm.* **64**, 180301 (2001).

[8] G.C. Dente and M.L. Tilton, J. Appl. Phys. **86**, 1420 (1999).

[9] G.C. Dente and M.L. Tilton, private communication, parabolicity α is defined by $E(1+\alpha E)=(hk)^2/2m_{\|}$.

[10] A.P. Ongstad, G.C. Dente, M.L. Tilton, D. Gianardi, and G. Turner, J. Appl. Phys. **87**, 7896 (2000).

[11] G. Liu and S.-L. Chuang, Phys. Rev. B **65**, 165220 (2002).

[12] D.–J. Jang, J.T. Olesberg, M.E. Flatte, T.F. Boggess and T.C. Hasenberg, Appl. Phys. Lett. **70**, 1125 (1997).

[13] O. Madelung, editor; Semiconductors: Group IV Elements and III-V Compounds" Springer-Verlag (1991).

[14] D.G. Cahill, W.K. Ford, K.E. Goodson, G.D. Mahan, A. Majumdar, H.J. Maris, R. Merlin, S.R. Phillpot, J. Appl. Phys. **93**, 793 (2003).

[15] D.-J. jang, M.E. Flatte, C.H. Grien, J.T. Olesberg, T.C. Hansberg, T.F. Boggess, Phys. Rev. B **58**, 13047 (1998).

Figure Captions

FIG. 1. The sum frequency spectra for different lattice temperatures at low carrier injection ($Pu = Pu_o/5$) and 250 ps probe delay.

FIG. 2. Measured crossing point from Fig. 1 and the calculated crossing energy as a function carrier temperature for density independent matrix element and for a matrix element proportional to $N^{0.17}$, simulating a type-II quantum well. Lines are only a guide for the eye.

FIG. 3. The linear and sum frequency spectra measured (thick faint lines) at 10 K and 250 ps probe delay for three injected densities (Pu_o, $Pu_o/2$ and $Pu_o/5$). The thin line traces are the interband transition only simulated spectra, and the dotted traces represents the simulation taking into account both the intervalence and interband transitions.

FIG. 4. Schematic figure of the band structure showing the interband (α_{cv}) transition and the intevalence (α_{IVA}) transition. The intervalence absorption energy spread (Δ_{IVA}) would be determined by the curvature of the deep hole band where IVA originates.

FIG. 5. The in-phase (dark line) signal representing the injection carrier contribution and quadrature (faint line) signals representing lattice heating measured at a delay of 250 ps for temperatures 80 K (a) and 180 K (b).

FIG. 6. Buildup and recovery of the thermal contribution to the transmission signal is plotted for different lattice temperatures. Traces were averaged in a digital scope and were recorded at a negative delay and at ~ 50 meV above the band edge. The extracted diffusion time constant is plotted in the inset. The pump was modulated with an acousto-optic modulator.

Figure 1

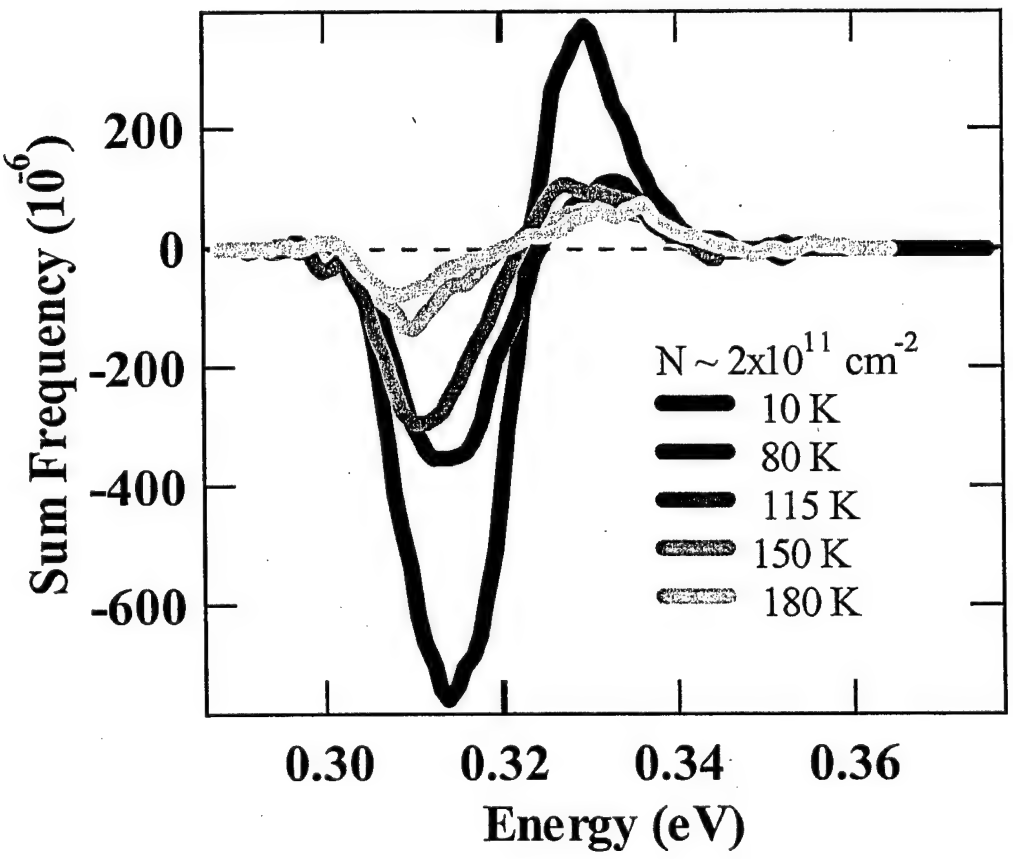
Sum Frequency (10^{-6})
200
0
-200
-400
-600
0.30
0.32
0.34
0.36
Energy (eV)
N ~ 2x10^{11} cm^{-2}
10 K
80 K
115 K
150 K
180 K

Figure 2

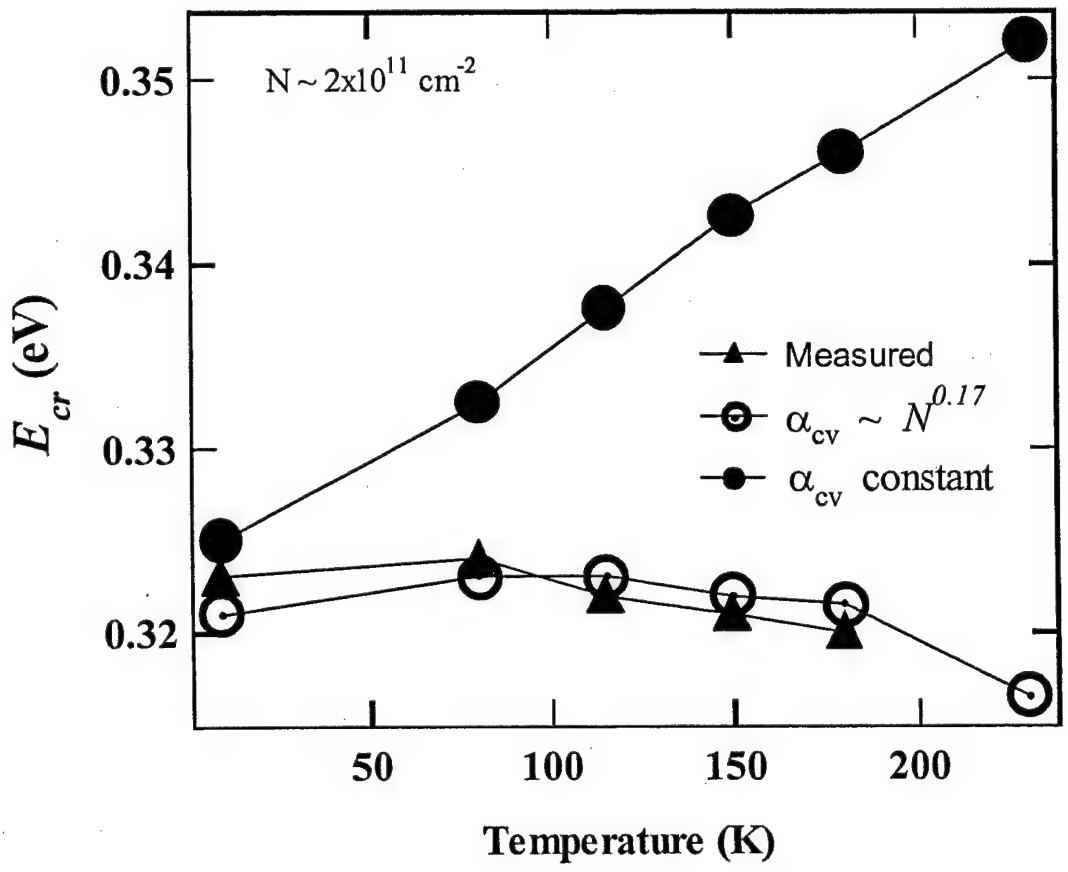
N ~ 2x10^11 cm^-2
0.35
0.34
0.33
0.32
E_cr (eV)
50
100
150
200
Temperature (K)
Measured
α_cv ~ N^0.17
α_cv constant

Figure 3

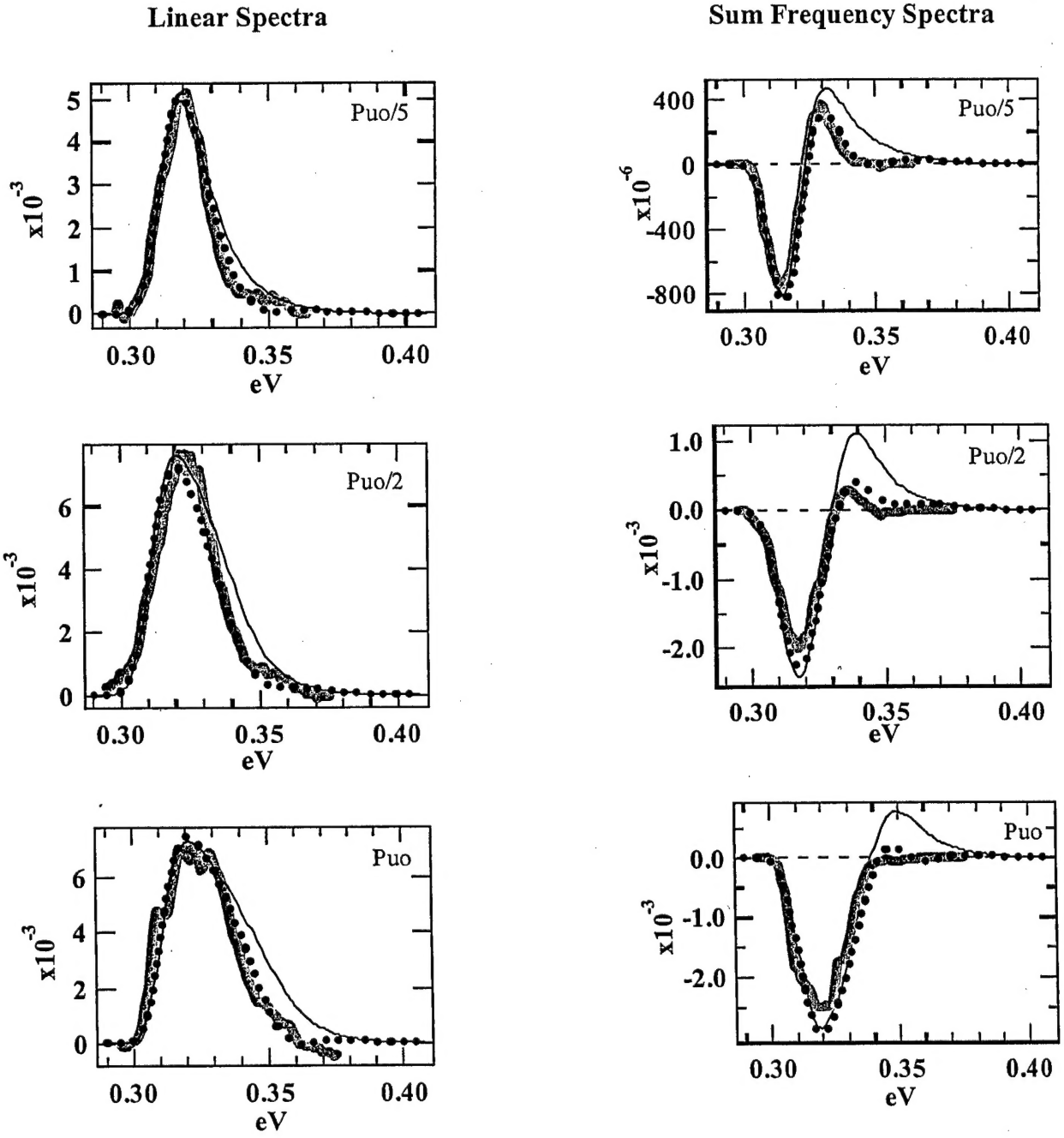
Linear Spectra
Sum Frequency Spectra
Puo/5
Puo/2
Puo
x10^-3
x10^-6
eV
0.30
0.35
0.40

Figure 4

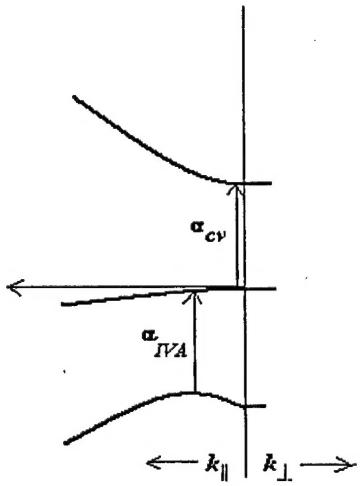

Figure 5

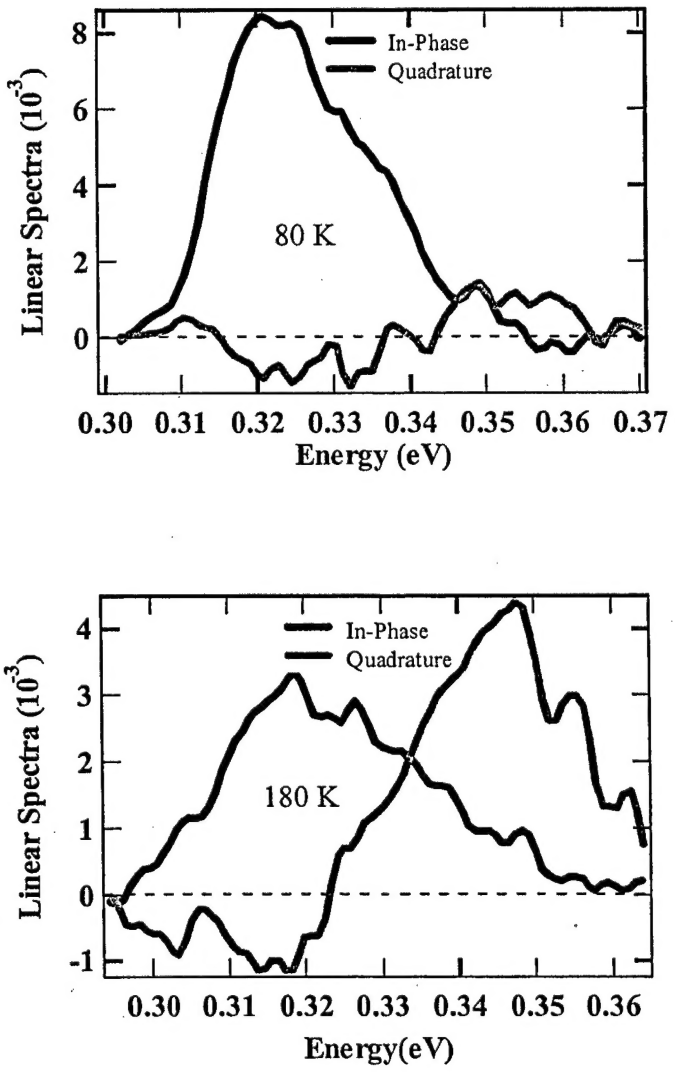
In-Phase
Quadrature
80 K
Linear Spectra (10^{-3})
8
6
4
2
0
0.30 0.31 0.32 0.33 0.34 0.35 0.36 0.37
Energy (eV)
In-Phase
Quadrature
180 K
Linear Spectra (10^{-3})
4
3
2
1
0
-1
0.30 0.31 0.32 0.33 0.34 0.35 0.36
Energy(eV)

Figure 6

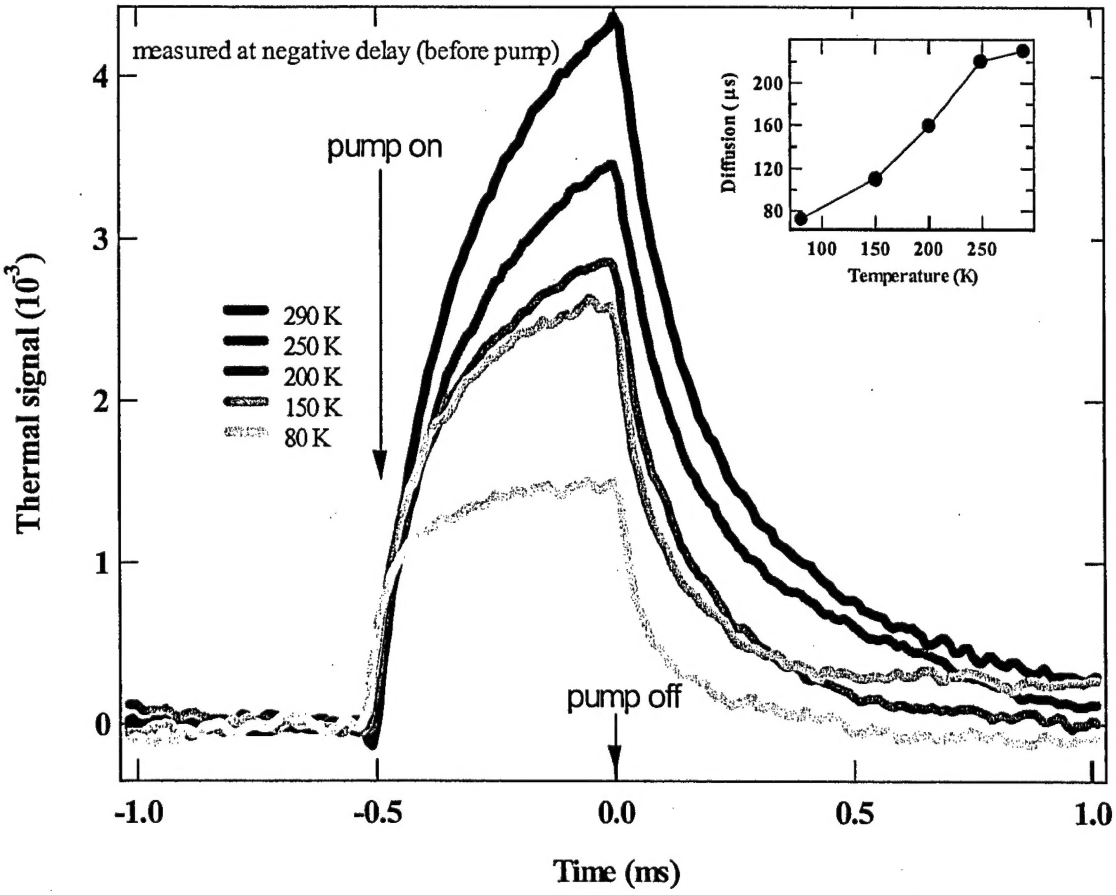
measured at negative delay (before pump)
pump on
pump off
290 K
250 K
200 K
150 K
80 K
Thermal signal (10^{-3})
Time (ms)
Diffusion (μs)
Temperature (K)